Surface Modification of Ti-6Al-4V Alloy with a Low-Energy, High-Current Electron Beam at Elevated Initial Temperatures[1]

V.P. Rotshtein, A.B. Markov, D.I. Proskurovsky, R. Günzel*, M. Pham**, E. Richter**, N. Shevchenko**, V.A. Shulov***, A.P. Rubshtein****

Institute of High-Current Electronics, 2/3, Akademichesky Ave., Tomsk, 634055, Russia, Phone (3822)491695, Fax (3822)492410, e-mail: Rvp@Lve.hcei.tsc.ru

** APT GmbH, Bautzner Landstr. 45, Gro?erkmannsdorf, 01454, Germany*

***Forschungszentrum Rossendorf e. V., Institute of Ion Beam Physics and Materials Research, P.O.B. 51 01 19, Dresden, 01314, Germany*

**** Moscow State Aviation Institute, 4, Volokolamskoe Shosse, Moscow, 125871, Russia*

*****Institute of Metal Physics, 18, S. Kovalevskaya St., Ekaterinburg, GSP-170, 620219, Russia*

Abstract – Surface topography, evolution of chemical and phase composition of the surface layers of Ti-6Al-4V alloy subjected to multiple pulsed electron-beam melting at the initial temperature of the target T_0 ranging from 20 to 550 °C have been investigated using optical, laser microscopy, SEM/EDS, AES and XRD analyses. Pulsed melting was induced by a low-energy (~20 keV), high-current electron beam (3 μs, 2.5 J/cm²). At T_0≤200 °C the cleaning of the near-surface layer from oxygen takes place. In contrast, at T_0≥400 °C a 1-μm thick surface layer quenched from the melt is enriched with oxygen from the residual gases of vacuum chamber. An increase in the initial temperature leads to a decrease in the residual stresses induced by pulsed heating. At T_0≤200 °C the martensite α′- and α″-phases are formed whereas at T_0=550 °C the ω-phase in the surface layers occurs. Surface microhardness increases with increasing the initial temperature and reaches 5 GPa at 550 °C. Wear resistance depends on the initial temperature non-monotonically: at T_0≤400 °C the wear resistance decreases but at T_0≤550 °C and at T_0=20 °C followed by vacuum annealing it increases up to 50-fold. Throughout the range of T_0 the pulsed melting results in the enhancement of corrosion resistance. The influence of initial temperature on the microstructure and properties of the surface layers are discussed based on the results of temperature field predictions.

1. Introduction

The pulsed surface melting of titanium alloys with a low-energy (~20 keV), high-current electron beam (LEHCEB) of microsecond duration followed by vacuum annealing, as shown in Refs. [1–3], allows cleaning the surface layer from the oxygen and carbon impurities, an increase in the aluminum content in the surface layer, and decreasing the surface roughness after grinding. The irradiation leads to the undesirable effects also, namely, to the surface cratering and the occurring of tensile stresses. Nevertheless, the multiply pulsed melting followed by vacuum annealing allows enhancing the strength and fatigue properties of Ti alloys.

The major cause of the cratering is the local overheating followed by melting of secondary-phase particles. The residual tensile stresses are caused by the high gradients of temperature in the surface layers during cooling [4, 5]. These effects can be effectively suppressed by increasing the lifetime of the melt and by reduction of the temperature gradients. This could be done by means of an increase in the pulse duration of e-beam and/or an increase in the initial temperature of irradiated material. The latter approach is much simply to realize in practice. Moreover, one can expect that this approach will allow excluding the procedure of the following vacuum annealing.

The objective of this research is to examine the effect of pulsed e-beam melting at elevated initial temperatures of a target on surface topography, chemical and phase compositions, microhardness, wear resistance and corrosion behavior of Ti-6Al-4V alloy.

2. Experimental

Flat samples 2÷5 mm thick and 20 mm in diameter made of Ti-6.1Al-4.4V (wt. %) alloy were preliminary annealed (920 °C, 2 h) and aged (550 °C, 4 h). The mirror polished samples were multiple irradiated with a LEHCEB in the initial surface melting mode: pulse duration τ=3 μs, energy density E_s=2.5 J/cm², number of shots N=40, and repetition rate 0.1 Hz [1–3].

The LEHCEB's source chamber was preliminary pumped using a turbomolecular pump up to a pressure of ~10^{-4} Pa. Samples were irradiated in Ar plasma at a pressure of $3\cdot10^{-2}$ Pa. The heater made of NiCr wire was located just behind the irradiated sample. The initial temperature of irradiated samples

[1] The work was supported by WTZ Project No. RUS 02/002

T_0 was 20, 200, 400 and 550 °C. After irradiation the sample initial temperature T_0 was hold for 5 min. During this time an inlet of Ar was stopped, the chamber was pumped up to a pressure of ~10^{-4} Pa whereupon the heater was switched off. After cooling of the sample down to 200 °C the pumping was stopped, and then the sample was cooling down to a room temperature at a pressure of <10^{-1} Pa. Some samples irradiated at 20 °C were subjected to the subsequent vacuum annealing (10^{-4} Pa, 550 °C, 2 h). All treatment modes of the samples are given in Table 1.

Table 1. Treatment modes of Ti-6Al-4V alloy

Treatment mode	Initial temperature, °C	Post-irradiation annealing
I	20	–
II	200	–
III	400	–
IV	550	–
V	20	+

The surface topography was examined with a scanning electron microscope (SEM, Hitachi), laser microscope (Keyence VK-8510), and profilograph (Dektak). The point chemical composition of the near-surface layers was determined from EDX spectra at accelerating voltage of 20 kV. The element profiles were determined by Auger electron spectroscopy (AES) using a Microlab 310F system.

The phase composition of the surface layers was examined by grazing incident X-ray diffraction (GIXRD) analysis at an incident angle of 1÷8° using D5000 type diffractometer as well as by X-Ray diffraction (XRD) analysis in Bragg-Brentano geometry using D8 (BRUKER AXS) type diffractometer with Cu K_α radiation. The thickness of an analysed layer for Ti target was 0.1÷1.5 μm for GIXRD and 8÷10 μm for XRD analysis [6].

The surface microhardness as well as microhardness depth profiles were measured by instrument of PMT-3 type at loads of 10, 20 and 50 g. The wear tests were performed at dry friction using the tribometer designed at Forschungszentrum Rossendorf under conditions as follows: 60 g a load applied to the indenter (a ball of 5 mm in diameter, steel 100 Cr6), 0.015 m/s sliding rate, 2 mm sliding track length, 1000÷10000 friction cycles. The wear volume of material was evaluated from the wear track profile. The wear volume of an indenter was determined also.

The corrosion behaviour was studied by potentiodynamic method (potentiostat of type AutoLab PGSTAT 12) in 1 % solution NaCl at a room temperature and potential variation rate 10 mV/s.

3. Results and discussion

3.1. Temperature fields

The method of calculations was described in detail elsewhere [5, 7]. Predictions have shown that at τ=3 μs the threshold of the surface melting of the Ti6Al-4V alloy is achieved at E_s=2÷2.5 J/cm^2, that agrees with experiment. Since the targets were multiple irradiated there is dispersion in energy density from one shot to another and thereby a maximum energy density in a series of pulses is larger than its average value. In our case, a maximum energy density is appeared to be 3.25 J/cm^2 which is 1.3 times that of the average value [8]. According to the calculations, at E_s=3.25 J/cm^2 an increase in the temperature T_0 in the range of 20÷550 °C leads to an increase in the melt thickness in the range of 1.5÷2.5 μm. At that a lifetime of the melt increases from 2.4 to 5.1 μs.

Metallographic examination of the irradiated samples has shown that as a result of a high-rate quenching from the melt the weekly-etched surface layer is formed. The thickness of this layer is 2÷3 μm that is in a good agreement with predictions of the melted layer thick.

In Fig. 1 the calculated temperature gradient profiles for the targets irradiated at various T_0 are presented. Curves correspond to the time the surface is being cooled down to 780 °C. As it can be seen an increase in the temperature T_0 leads to an decrease in the temperature gradient within the heat affected zone (HAZ) by two orders of magnitude. So, the rise in the target initial temperature has to lead to a significant decrease both the quasi-static [4, 5] and the residual stresses within HAZ.

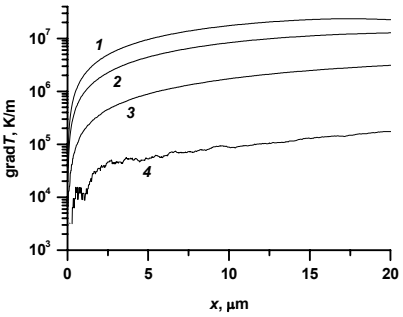

Fig. 1. Profiles of temperature gradients of Ti-6Al-4V alloy target irradiated at 3.25 J/cm^2 at various temperatures T_0: (1) 20, (2) 200, (3) 400 and (4) 550 °C

3.2. Surface topography

Non-irradiated Ti-4Al-4V alloy contains the globular grains of α-phase with an average size of 5 μm divided by interlayers of β-phase. As follows from SEM observations (see Fig. 2, *a*), the multiple surface melting leads to weakening the contrast ratio caused by presence of two phases. It testifies to an decrease in the content of β-phase due to high-rate quenching from the melt. At T_0=20 and 200 °C the lamellar microrelief is formed in grains (Fig. 2, *a*). Its occurrence can be associated, first, with martensite transformation in the (α+β) Ti alloys quenched from β-field (as will be shown in Sec. 3.4), secondly, with a plastic deformation caused by the compressive (in a surface plane) quasi-static stresses [4, 5], thirdly, with formation of secondary α-plates due to full de-

cay of a residual β-phase. The latter process is practically finished at T_0=400 °C that is why the secondary α-plates are not occurred in this case (Fig. 2, *b*).

The rare microcraters are observed at the irradiated surface similar to those described in Refs. [1, 2]. The cratering probability almost don't depend on T_0. Even for the microcraters of a large diameter of ~70 μm their depth does not exceed 2 μm, i.e. the microcraters are not deep. According to EDS, the microcrater bottom is enriched with oxygen that is in agreement with the data presented in Ref. [1].

The roughness of irradiated surface increases with increasing initial temperature T_0. This is caused by the anisotropy of the coefficient of thermal expansion of α-Ti [9]. When increasing T_0 the thickness of the HAZ increases. It leads to an increase in the deformation gradient of adjacent grains and consequently to an increase in the surface roughness. It should be pointed out that for all above-mentioned treatment modes the surface roughness R_a does not exceed 0.2 μm that is acceptable for many Ti-alloys applications.

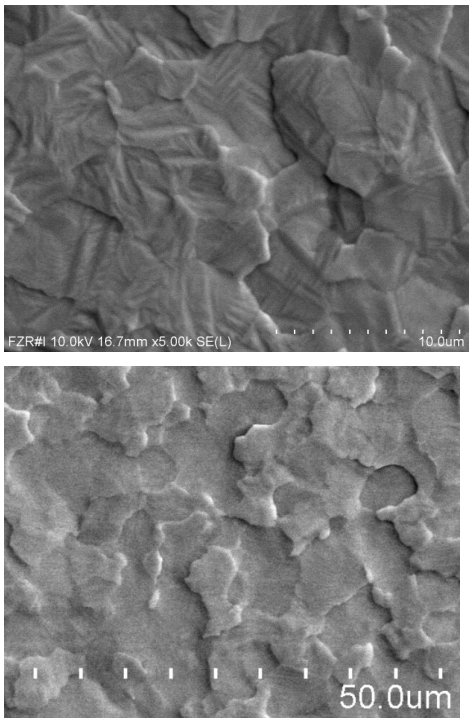

a

b

Fig. 2. SEM images of the surface of e-beam treated Ti-6Al-4V alloy at 20 (a) and 400 °C (b)

3.3. AES profiles

Fig. 3 shows the AES depth profiles of the non-irradiated and multiple irradiated at 20 °C Ti-6Al-4V alloy. The non-irradiated surface contains 50 at. % O and 20 at. % C. High oxygen content is caused by presence of native oxide film of TiO_2. After the irradiation at 20 and 200 °C an oxygen content at the surface decreases while carbon content, on contrast, increases up to 25÷33 % (see Figs. 3 and 4). The latter result can be explained as follows. Oxygen and carbon are supplied at the irradiated surface from the residual gases of vacuum chamber. Just after irradiation the surface is oxygen-free during some time. However, its roughness is higher than that of the non-irradiated surface. That is why such the surface can absorb the higher carbon content from the residual environment before it will be covered by oxide film.

In the initial state the thickness of the near-surface layer enriched with oxygen is reached about 40 nm (see Fig. 3, *a*). After the irradiation at 20 and 200 °C the thickness of this layer decreases by a factor of 2 (Figs. 3 and 4) that points to cleaning the surface from oxygen in this treatment modes. At $T_0 \geq 400$ °C, in contrast, the enrichment of near-surface layer with oxygen occurs; herewith, oxygen content at the depth of x>400 nm is higher than the vanadium content.

Post-irradiation vacuum annealing (mode V) leads to even higher enrichment of the near-surface layer with oxygen (Fig. 4). Obviously, it is associated with the diffusion of oxygen from a residual gases at elevated temperatures and long-lasting exposure. It should be noted that the multiple pulsed melting can accelerate a diffusivity of oxygen due to increasing the concentration of quenched vacancies and dislocation density in the surface layer [4, 5].

As follows from AES, the depth profiles of carbon are limited to 10 nm. These profiles are similar to each other and almost don't depend on the temperature T_0.

3.4. XRD analysis

GIXRD analysis the near-surface layer of thickness up to 1.5 μm, which was quenched from the melt, while XRD examines also the deeper layers (of thickness up to 10 μm) which had not been melted and where the solid-state transformations may occur.

According to XRD patterns (see Fig. 5) the non-treated Ti-6Al-4V alloy contains reflections of α-and β-phases. After irradiation at 20 and 200 °C (modes I and II) the broadening of α-phase reflections and its shifting towards the larger angles 2θ are observed. It points to the formation of martensite α'-phase, increasing the microstresses, and formation of residual tensile stresses, that is in agreement with the results obtained elsewhere [2].

After irradiation at 400 and 550 °C (modes III and IV) the broadening of α-phase reflections decreases noticeably, but they practically don't shift. Hence, an increase in the temperature T_0 leads to a decrease in the microstresses, the relaxation of the residual tensile stresses, and also the suppression of martensite transformation. The latter may be explained by the fact that the martensite $\beta \rightarrow \alpha'-$ transformation is incompleted at elevated initial temperatures. Suppression of this transformation at elevated temperature T_0 testifies that the surface microrelief observed at T_0=20 °C (Fig. 2, *a*) and 200 °C is formed due to the martensite transformation.

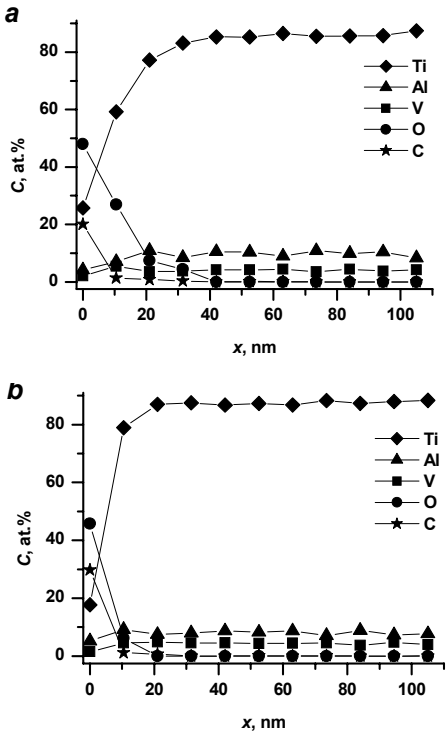

Fig. 3. AES depth profiles of non-irradiated (a) and e-beam irradiated at 20 °C (b) Ti-6Al-4V alloy

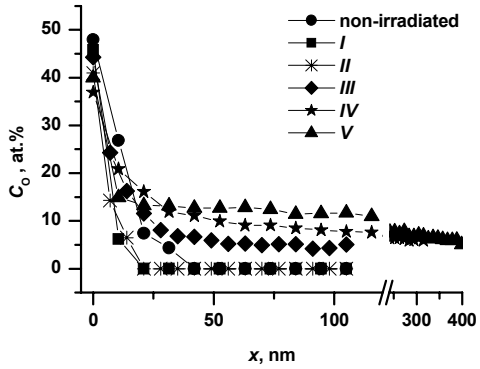

Fig. 4. AES oxygen depth profiles of Ti-6Al-4V alloy for various treatment modes

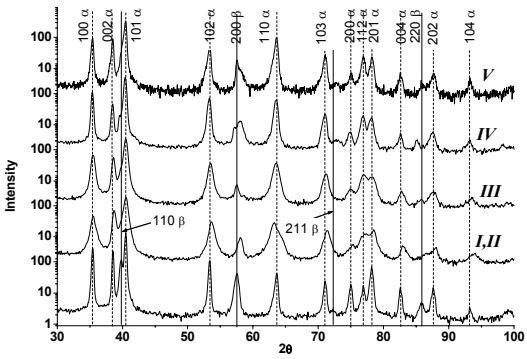

Fig. 5. XRD patterns of Ti-6Al-4V alloy in initial state (bottom) and after e-beam treatment in various modes (I–V)

Post-irradiation vacuum annealing (mode V) acts similar to irradiation at 550 °C (mode IV) resulting in the relaxation of micro- and macrostresses as well as decay of martensite α'-phase. These data are in a good agreement with the results obtained elsewhere [2].

In all irradiation modes the reflections of β-phase are presented in XRD patterns, however, their intensity is noticeably lower, than that of the non-irradiated sample. For IV and V modes the broadening of reflection of (200) β-phase and its splitting takes place that is evidence of ω-phase formation owing to $\beta \rightarrow \omega$ – transformation. Note, that the formation of ω-phase under quenching results in the strengthening of ($\alpha+\beta$) Ti alloys [10].

GIXRD examinations have shown, that the diffraction patterns are almost independent on the angle ω in a range of 1÷8°. Fig. 6 shows the diffraction patterns for various treatment modes obtained at ω=1° which corresponding to a thickness of analyzed layer of 0.1÷0.2 μm. At a temperature T_0=20 and 200 °C (modes I and II) as distinct from the others treatment modes, at all angles the splitting of (110) α-phase reflections occurs that is evidence of $\alpha' \rightarrow \alpha''$ – transformation. Formation of α''-martensite phase leads to a decrease in the strength and an increase in the ductility of ($\alpha+\beta$) Ti alloys [10].

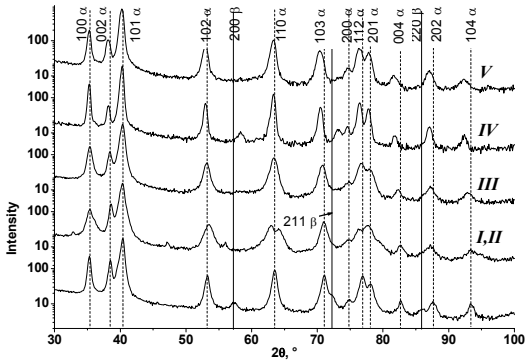

Fig. 6. GIXRD patterns (ω=1°) of Ti-6Al-4V alloy in initial state (bottom) and after e-beam treatment in various modes (I–V)

Reflections of β-phase are observed after irradiation at T_0=550 °C (mode IV) at all angles ω. Besides, these reflections exist after pulsed melting at 20 °C followed by annealing (mode V) but only at ω=4 and 8°. In other cases the reflections of β-phase are absent. Comparing these data with the above described results it can be deduced that β-phase observed at T_0=20 and 200 °C (modes I and II) in Bragg-Brentano geometry is located underneath the surface layer quenched from the melt.

3.5. Microhardness tests

The surface microhardness for the various treatment modes is given in Table 2. As shown, the microhardness increases monotonically with increasing the temperature T_0 and at 550 °C it reaches ~5 GPa

that is almost 2 times higher than that of untreated material. After multiple pulsed melting followed by vacuum annealing (mode V) a microhardness is close to that obtained at 400 °C (mode III). It should be noted that since a penetration depth of indenter is more than 1.5÷2 μm the microhardness values correspond to the surface layers both quenched from the melt and subjected to the pulsed heating in a solid phase.

Table 2. Surface microhardness of Ti-6Al-4V alloy for various treatment modes

Treat-ment mode	Microhardness, GPa		
	P=0.1 N	P=0.2 N	P=0.5 N
Non-treated	2.5±0.2	2.8±0.2	3.0±0.2
I	3.6±0.2	3.4±0.2	2.9±0.2
II	4.1±0.3	3.3±0.3	3.7±0.3
III	4.3±0.3	4.8±0.3	4.1±0.3
IV	5.7±0.3	5.0±0.3	4.7±0.3
V	3.8±0.3	4.1±0.3	4.6±0.3

It can be seen from XRD analysis that an increase in the surface microhardness is associated with the relaxation of residual stresses induced at pulse heating and the formation of ω-phase (modes IV and V). Besides, as it follows from AES analysis, the increase in microhardness may take place due to formation of precipitations of TiO_2 type as a result of absorption of oxygen atoms by a surface heated up to a high temperatures (precipitation hardening), as well as due to increase in oxygen content in the α-solid solution (solid-solution hardening).

The in-depth microhardness measurements have shown that regardless of T_0 the microhardness decreases with distance from the irradiated surface and reaches the original value at the depth of ~50 μm. Thus, a thickness of the hardening layer is limited by HAZ.

3.6. Wear resistance

As can been seen from Fig. 7, irradiation at T_0≤400 °C (modes I–III) leads to a decrease in the wear resistance of Ti-6Al-4V alloy compared to that of non-irradiated samples (see Fig. 7). The maximal wear (the top right point in Fig. 7) corresponds to track depth of 18 m, i.e. a wear is occurred within the HAZ. Increased wear of irradiated samples is probably due to the residual tensile stresses formed in the surface layer after irradiation. In contrast, the irradiation at 550 °C (mode IV) and at 20 °C followed by vacuum annealing (mode V) leads to a significant increase in the wear resistance. In a mode IV for the maximal sliding distance the wear resistance of Ti-6Al-4V alloy increased by a factor of 50 when compared with that of untreated sample (Fig. 7), and in mode V no evidence of wear was found. However, in these two modes the noticeable wear of steel indenter was observed. Enhancement of wear resistance of Ti-6Al-4V alloy treated in IV and V agrees with the formation of ω-phase as well as with noticeable increasing in the surface microhardness.

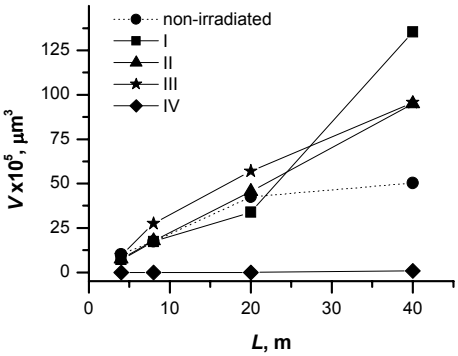

Fig. 7. Volume wear of Ti-6Al-4V alloy as a function of sliding distance for various treatment modes

3.7. Corrosion behavior

Fig. 8 shows anode polarization curves of untreated and e-beam-treated samples. The curves corresponding to the treatment modes I and II are practically coincide. As it can be seen after irradiation the current density decreases more than one order of magnitude that is evidence of increase in the corrosion resistance. This result agrees with the results of Ref. [11]. Moreover, there is an agreement between the enhanced corrosion resistance and formation of "white" layer at the irradiated surface after chemical etching.

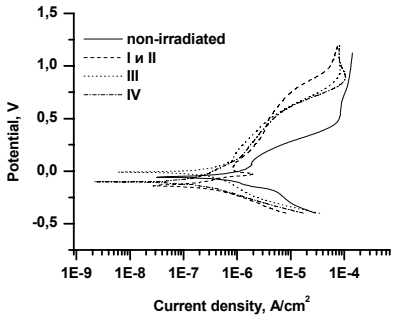

Fig. 8. Anode polarization curves of Ti-6Al-4V alloy in 1 % NaCl solution for various treatment modes

4. Conclusions

1. Simulations showed that an increase in the initial temperature (up to T_0=550 °C) of Ti-6Al-4V target irradiated with a LEHCEB in the initial surface melting mode leads to an increase in the melt thickness from 1.5 to 2.5 μm and a decrease in the temperature gradients within HAZ by 2 orders of magnitude.
2. Multiple pulsed melting at T_0≤200 °C results in cleaning the near-surface layer from oxygen. Similar treatment at 400 and 550 °C as well as at 20 °C followed by vacuum annealing leads to an increase in the oxygen content in the near-surface layer quenched from the melt due to its absorption from a residual gases of vacuum chamber.
3. At T_0≤200 °C the martensite α'- and α''-phases are formed in the surface layer quenched from the

melt. At T_0=550 °C the formation of the ω-phase takes place. An increase in the temperature T_0 leads to a decrease in the residual stresses in the surface layer formed at pulsed heating.

4. Microhardness of the surface layer quenched from the melt as well as deeper layers increases monotonically with increasing T_0. Surface hardening at 400 and 550 °C may take place due to the formation of both ω-phase and disperse TiO_2 particles which may occur as a result of oxygen enrichment.
5. Wear resistance of the Ti-6Al-4V alloy depends on T_0 non-monotonically. At $T_0 \leq 400$ °C the irradiation leads to a decrease in the wear resistance that may be explained by formation of residual tensile stresses after irradiation. Irradiation at 550 °C as well as at 20 °C followed by vacuum annealing leads to the significant (by a factor of 50) increase in the wear resistance. This effect agrees with formation of ω-phase and noticeable increasing the microhardness.
6. Multiple pulsed melting enhances the corrosion resistance of the Ti-6Al-4V alloy regardless of initial temperature of the target.

The authors would like to thank K. Karlik for the irradiation of samples.

References

[1] N.A. Nochovnaya, V.A. Shulov, V.P. Rotshtein, A.B. Markov, S.D. Nazarov, G.E. Ozur, D.I. Proskurovsky, *in Proc. 5th Intern. Conf. on Electron Beam Technology (EBT-97)*, Varna, Bulgaria, 1997, pp. 215–220.

[2] N.A. Nochovnaya, V.A. Shulov, D.S. Nazarov, G.E. Ozur, D.I. Proskurovsky, V.P. Rotshtein, I.G. Karpova, Rus. Fizika i Himiya Obrabotki Materialov, 1, 27 (1998).

[3] D. Proskurovsky, V. Rotshtein, G. Ozur, A. Markov, D. Nazarov, V. Shulov, Yu. Ivanov, R. Buchheit, J. Vac. Sci. Technol. A 16 (4) 2440 (1998).

[4] D.I. Proskurovsky, V.P. Rotshtein, G.E. Ozur, Yu.F. Ivanov, A.B. Markov, Surf. and Coat. Technol., 125, 49 (2000).

[5] V. Rotshtein, Yu. Ivanov, A. Markov. Chapter 6 in book "Materials surface processing by directed energy techniques" p. 205–240. Ed. by Y. Pauleau, Elsevier, 2006, 736 p.

[6] B.L. Henke, E.M. Gullikson, and J.C. Davis, Atomic Data and Nuclear Data Tables, 54 (2), 181 (1993).

[7] A.B. Markov, V.P. Rotshtein, Nucl. Inststr. and Meth. in Phys. Res. B, 132, 79 (1997).

[8] A.B. Markov, V.P. Rotshtein, High Temperature. 38 (1) 15 (2000).

[9] U. Zwicker. *Titan und Titanlegierungen*, Springer-Verlag, Berlin, 1974.

[10] O.P. Solonina, S.G. Glazunov, *Heat-resistance titanium alloys*. Moscow, Metallurgy, 1976, p. 447.

[11] P. Roharjo, K. Uemura, A. Okada, Y. Uno, *in Proc 7th Int. Conf. on Modification of Materials with Particle Beams and Plasma Flows*, Tomsk, Russia, 2004, pp. 267–270.